# Ionic relaxation contribution to the electronic reconstruction at the *n*-type $LaAlO_3/SrTiO_3$ interface

Rossitza Pentcheva[1] and Warren E. Pickett[2]
[1]*Department of Earth and Environmental Sciences, University of Munich, Theresienstr 41, 80333 Munich, Germany*
[2]*Department of Physics, University of California, Davis, California 95616, USA*
(Received 30 June 2008; revised manuscript received 19 September 2008; published 7 November 2008)

Density-functional theory calculations reveal that the compensation mechanism at the isolated *n*-type interface in $LaAlO_3/SrTiO_3$ superlattices involves both ionic and electronic degrees of freedom. Strong polar distortions screen the local electric field and reduce the band discontinuity across the interface. We find that the electronic reconstruction depends sensitively on whether structural optimization is performed within GGA (conventional exchange and correlation effects) or GGA+$U$ (which includes strong intra-atomic interactions). For a structural optimization within GGA+$U$ the excess charge is confined to the interface $TiO_2$ layer with a charge-ordered, orbitally polarized arrangement of $Ti^{3+}$ and $Ti^{4+}$. While the charge-ordered phase represents the ground state, optimization within GGA leads to more pronounced lattice polarization, suppression of charge order (with remaining $d_{xy}$-orbital occupation in the interface layer), and a delocalization of the excess charge extending over a few $SrTiO_3$ layers.

DOI: 10.1103/PhysRevB.78.205106 PACS number(s): 73.20.Hb, 75.70.Cn, 71.28.+d

## I. INTRODUCTION

Correlated electrons in oxide heterostructures open up new possibilities for electronic behavior that is unanticipated from the properties of the bulk constituents and can thus lead to new functionality. Although $SrTiO_3$ (STO) and $LaAlO_3$ (LAO) are two conventional nonmagnetic band insulators, their interfaces were reported to be conducting.[1] Recently, there are indications for magnetism[2,3] and superconductivity[4] in this system at low temperature. These new functionalities lend extra urgency to the effort to understand the unanticipated properties of this interface.

In the perovskite structure there is a natural charge modulation in the [001] direction; e.g., in $LaAlO_3$ positively charged LaO layers alternate with negatively charged $AlO_2$ layers, while in $SrTiO_3$ both the SrO and $TiO_2$ layers are charge neutral. At both interfaces, the electron-doped *n*-type ($LaO/TiO_2$) and the hole-doped *p*-type ($AlO_2/SrO$), local charge neutrality as inferred from the formal valences is disrupted. This violation of charge neutrality turns out to be a driving force toward the unexpected behavior emerging at the interface.

Theoretical studies so far concentrate on explaining the reported conductivity in this system (e.g., Refs. 5–7) by considering the ideal (defect-free) interface. However, on the experimental side there is meanwhile a consensus that the oxygen pressure during growth and post annealing plays a crucial role. The initially measured high conductivity is attributed to oxygen defects rather than being an intrinsic property.[8–12] Rijnders and Blank[13] related recently the three novel functional properties to three regions of oxygen pressure: (i) high conductivity is measured in samples grown at or below $p_{O_2} \sim 10^{-6}$ mbar oxygen pressure in the chamber; (ii) superconductivity was found for intermediate pressures of $p_{O_2} \sim 10^{-4}-10^{-5}$ mbar; (iii) magnetism and nonconducting behavior were observed only for $p_{O_2} \sim 10^{-3}$ mbar. The higher oxygen pressure is widely thought to mitigate the formation of oxygen vacancies, resulting in more nearly stoichiometric materials.

In this paper we concentrate on the intrinsic effects in the case where the influence of oxygen defects is minimized and study the (effectively) isolated *n*-type interface. Using density-functional theory (DFT) calculations and including a Hubbard $U$ we have found previously that the charge mismatch at the *n*-type LAO/STO interface is accommodated by charge disproportionation on the Ti sublattice in the interface layer with $Ti^{3+}$ and $Ti^{4+}$ ordered in a checkerboard arrangement.[14] This diluted layer of $Ti^{3+}$ spins shows a slight preference for antiferromagnetic coupling,[15] as found also for $LaTiO_3/SrTiO_3$ superlattices.[16] First experimental indications for localized magnetic moments at the interface were obtained by Brinkman *et al.*[2] Because the above-mentioned calculations were done for a superlattice containing a single unit cell of each material and ideal (bulk) positions of the ions in the cell, we study here the compensation mechanism in more separated interfaces containing thicker slabs of both materials. We focus specifically on the crucial role of lattice relaxations on the electronic state at the interface, since the largest contribution to the static dielectric constant in both materials arises from the lattice response. In addition we explore how the level of treatment of correlation for the Ti 3*d* bands influences the structural and electronic properties at the interface. Finally, the band alignment across the interface is determined.

## II. CALCULATIONAL DETAILS

The DFT calculations are performed using the all-electron full-potential augmented plane-wave (FP-APW) method in the WIEN2K implementation[17] and the generalized gradient approximation (GGA) (Ref. 18) of the exchange-correlation potential. Because at the *n*-type interface a LaO layer is placed next to a $TiO_2$ layer which is the building unit of the Mott insulator $LaTiO_3$, we have considered an on-site Coulomb repulsion on the Ti 3*d* states within the fully localized limit (LDA+$U$) (Ref. 19) using $U=8$ eV and $J=1$ eV. These values are necessary to describe the insulating nature

 

of undistorted bulk $LaTiO_3$.[20] Additionally, $U=7.5$ eV is used to shift the unoccupied La $f$ states to higher energies. However, due to the localized nature of the $f$ states this does not influence qualitatively the electronic behavior of the system. The muffin-tin (MT) radii are as follows: $R^{MT}_{La,Sr}=2.30$ bohr, $R^{MT}_{Ti,Al}=1.80$ bohr, and $R^{MT}_{O}=1.60$ bohr. We use a mixed APW+lo and LAPW basis set with the following convergence parameters: Inside the muffin tins wave functions are expanded in spherical harmonics up to $l^{wf}_{max}=10$ and nonspherical contributions to the electron density and potential up to $l^{pot}_{max}=6$ are used. The energy cutoff for the plane-wave representation in the interstitial is $E^{wf}_{max}=19$ Ry for the wave functions and $E^{pot}_{max}=196$ Ry for the potential.

To allow the possibility for more complex symmetry breaking and charge ordering, the calculations are performed in cells with a $c(2\times2)$-lateral periodicity and 15 $k$ points in the irreducible part of the Brillouin zone. We have used the lateral lattice constant of the $SrTiO_3$ substrate obtained from GGA (3.92 Å) and $c=10a$. We note that other studies[5–7] have used LDA together with the LDA lattice parameter (3.84 Å), but we choose here the GGA value also because it is in closer agreement with the experimental lattice constant (3.905 Å). Thus the $LaAlO_3$ film (3.79 Å) is subject to tensile strain on $SrTiO_3$ due to a lattice mismatch of 3%. In order to avoid the formation of a nonperiodic potential in an asymmetric setup, the superlattice (SL) is modeled by a symmetric supercell containing two $n$-type interfaces. To explore the effect of treatment of electronic correlations on the structural properties a full structural optimization of the internal parameters within the tetragonal unit cell was performed both within GGA and GGA+$U$.[21]

## III. IONIC RELAXATIONS

While previous studies concentrated on superlattices containing one,[14] two,[6,15] and four[5] unit cells of each material, here we investigate the compensation mechanisms in more separated interfaces using a slab containing 4.5 and 5.5 unit cells of the respective bulk compounds as shown in Fig. 2. This system will be denoted as $LAO_{4.5}/STO_{5.5}$ in the following. Generally, displacements from the ideal structure due to strain should affect cations and anions equally, thus giving no lattice polarization. Effects that result in differing displacements for cations and anions have a polar character; i.e., they produce an electric field or are a response to an electric field, caused in the present case by the change mismatch across the interface.

The lattice relaxations obtained within GGA and GGA+$U$ are presented in Fig. 1. The biggest displacements are observed at the interface where the differences in electronic distribution are largest. Generally, within GGA+$U$ the relaxations are smaller than within GGA and confined closer to the interface (IF) with the displacements being more pronounced on the LAO side compared to the STO side. Within GGA, oxygen relaxations are more symmetric across the interface. While both Ti and O in the interface $TiO_2$ layer move toward the LaO layer, the shifts are stronger for oxygen (0.32 Å for GGA; 0.22 Å for GGA+$U$), leading to a distinct layer polarization of 0.17 Å (GGA) and 0.12 Å

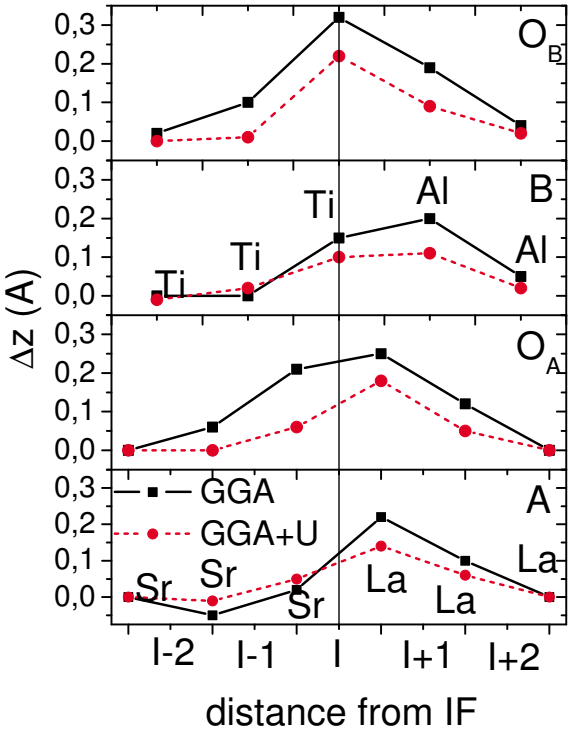


FIG. 1. (Color online) Vertical displacements of ions $\Delta z$ in Å in the $LAO_{4.5}/STO_{5.5}$ superlattice with respect to the bulk positions obtained within GGA (solid black line) and GGA+$U$ (red dashed line). The $x$ axis shows the distance from the interface (I) $TiO_2$ layer. A, B, $O_A$, $O_B$ denote the positions of ions in the layered $ABO_3$ perovskite lattice.

(GGA+$U$). These values are similar to ferroelectriclike distortions found in the interface $TiO_2$ layer in LTO/STO superlattices[22,23] although the direction of Ti displacement is opposite, which we attribute to the different sign of lattice mismatch. Taking into account the ionic charges, the polar distortions correspond to a layer-resolved dipole per interface of −0.68 eÅ (GGA) and −0.48 eÅ (GGA+$U$) and a change in potential across the interface $TiO_2$ layer of 0.70 eV (GGA) and 0.45 eV (GGA+$U$).

Within GGA polar distortions are observed also in the SrO layer next to the interface, where the Sr ion remains nearly at its bulk position while the oxygen moves toward the interface by 0.21 Å leading to a ferroelectriclike shift between Sr and O of 0.19 Å. Because both La and O on the other side of the interface shift by 0.22 and 0.25 Å, respectively, the La-Sr separation is increased by 0.20 Å. This value agrees well with the 4.9% elongation inferred from a high-resolution transmission electron microscopy study.[24] While Maurice *et al.*[24] attributed this result to a stretching of the $TiO_6$ octahedron at the interface due to a Jahn-Teller effect, we find no indication for this as both apical oxygens shift by nearly the same amount (0.21 and 0.25 Å). On the other hand within GGA+$U$ the polar distortion is confined to the interface and an elongation of the $TiO_6$ octahedron of 0.12 Å is observed.

Strong relaxations at the interface were also obtained from pseudopotential calculations using a $LAO_{8.5}/STO_{8.5}$ superlattice.[25] DFT-GGA studies with smaller simulation

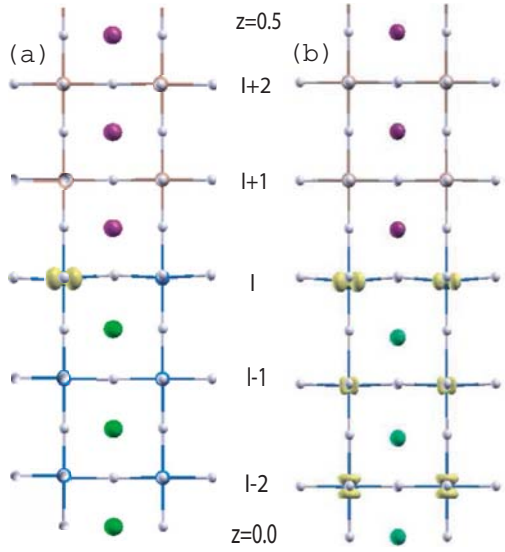


FIG. 2. (Color online) Crystal structure of a $LAO_{4.5}/STO_{5.5}$ superlattice showing half of the simulation cell with atomic relaxations obtained within (a) GGA+$U$ and (b) GGA. Additionally, the charge-density distribution of the occupied Ti 3$d$ states obtained for both geometries is displayed. For the geometry obtained within GGA+$U$ the Ti 3$d$ occupation is confined to the interface layer with $Ti^{3+}$ and $Ti^{4+}$ arranged in a $c(2\times2)$ manner with an occupied $d_{xy}$ orbital at the $Ti^{3+}$ sites. For (b) the strong polar distortions suppress charge order and delocalize the excess charge throughout the STO slab, while orbital order ($d_{xy}$ partial occupation) is retained in the interface layer.

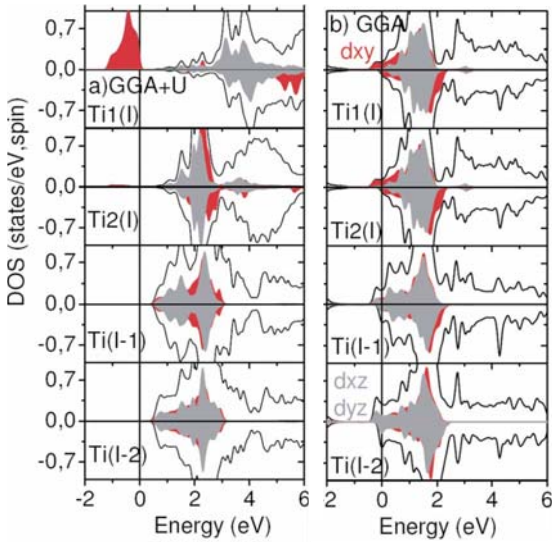


FIG. 3. (Color online) Layer-resolved density of states of a $LAO_{4.5}/STO_{5.5}$ SL obtained within GGA+$U$ with atomic positions relaxed within (a) GGA+$U$ and (b) GGA. The two topmost panels show the two Ti ions at the interface; the succeeding panels show the behavior of the Ti ions in deeper layers of the STO part of the slab. For the geometry obtained within GGA the excess charge is confined to the IF with a $Ti^{3+}$, $Ti^{4+}$ layer and rapid relaxation of the deeper layers toward bulk behavior. The structure relaxed within GGA leads to a metallic STO part, suppressed charge order and a residual orbital order ($d_{xy}$ –red/dark gray filling) at the Ti (I) sites and degenerate $t_{2g}$ states in deeper layers.

cells give qualitatively the same behavior but the actual values of interfacial buckling are smaller (0.02–0.10 Å) (Refs. 5 and 7) and the elongation of the $TiO_6$ octahedron is 2.9% (0.11 Å).[6] By reducing further the symmetry in a $LAO_{1.5}/STO_{2.5}$ supercell, Zhong and Kelly[15] found indications for an additional octahedron tilting.

## IV. ELECTRONIC RECONSTRUCTION

The differences in relaxations obtained within GGA and GGA+$U$ are closely related to the different compensation mechanism of the polar discontinuity at the interface. Here we discuss how relaxations influence the electronic properties. The checkerboard arrangement of $Ti^{3+}$ and $Ti^{4+}$ at the interface is found both in the $LAO_1/STO_1$ heterostructure studied previously[14] and the $LAO_{4.5}/STO_{5.5}$ superlattice for the ideal positions of the ions. The structural optimization performed within GGA+$U$ strengthens further the charge-ordered (CO) state. The spatial distribution of the occupied $d$ states in the interface $TiO_2$ layer in Fig. 2(a) shows a disproportionation in $Ti^{3+}$ and $Ti^{4+}$ with an occupied $d_{xy}$ orbital (and a magnetic moment of 0.76 $\mu_B$) at the $Ti^{3+}$ sites. Moreover, the lateral relaxation of oxygen by 0.04 Å away from $Ti^{3+}$(breathing mode) leads to a further localization of the excess electron and an increase of the gap between the lower Hubbard band ($d_{xy}$ orbital) and the unoccupied Ti 3$d$ orbitals from nearly zero to 0.3 eV as shown in the projected density of states (DOS) in Fig. 3(a).

For comparison we have performed a GGA+$U$ calculation using the geometry obtained in the GGA optimization. This configuration lies 0.45 eV above the CO ground state. We find that here the strong relaxations and polar distortions lead to a suppression of the charge ordering at the interface. As shown both in Figs. 2(b) and 3(b) the excess charge at the interface becomes more delocalized, resulting in partial occupation of the Ti 3$d$ bands in deeper layers on the STO side. This is in agreement with Hamann *et al.*,[22] who suggested that the lattice polarization at the IF acts to overscreen the charge in the LaO layer and reduce the trapping of the 2D electron gas at the interface. While at the interface the occupied Ti 3$d$ states still have $d_{xy}$ character, in deeper layers the $t_{2g}$ orbitals are degenerate. Still, the magnetic moments are almost identical (0.14 $\mu_B$) throughout the STO part.

Thus we find two distinct solutions resulting from a geometry optimization within GGA and GGA+$U$: a ground state where the excess charge is localized at the interface in a charge-ordered and orbitally polarized ($d_{xy}$) insulating state and an energetically higher solution showing stronger ferroelectriclike distortions resulting from the relaxation within GGA. In the latter case the charge order at the interface is suppressed and the excess charge is delocalized to several STO layers, and the system is metallic. This solution is consistent with other studies (GGA and GGA+$U$) using a (1 $\times$1) unit cell.[23,26] Samples grown at high oxygen pressures ($\sim10^{-3}$ mbar) show a sheet resistance at 5 K of 5 $\times10^4$ $\Omega/\square$ that is 7 orders of magnitude higher than the initially reported one at $p_{O_2}=10^{-6}$ mbar.[2] This suggests a

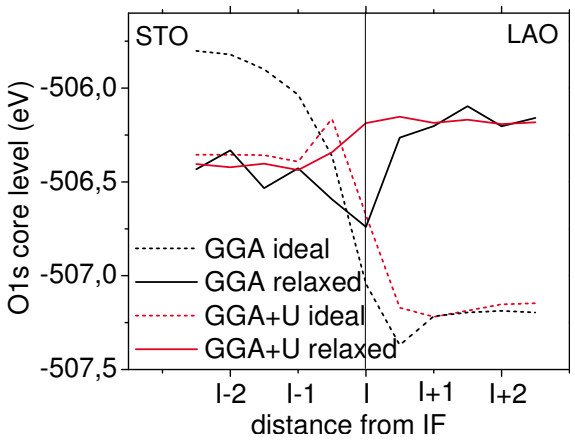


FIG. 4. (Color online) Positions of O 1*s* core levels (with respect to the Fermi level, $E_v$), across the interface in the $LAO_{4.5}/STO_{5.5}$ superlattice before (dashed) and after (solid) relaxation obtained within GGA (black line) and GGA+$U$ (red/dark gray line). The $x$ axis shows the distance from the interface (I) $TiO_2$ layer. The Fermi levels of all systems are set to zero and only relative variations of the O 1*s* levels from layer to layer are of interest.

(nearly) insulating ground state for high oxygen pressures. Moreover, $R_S$ exhibits a logarithmic decrease up to 50 K, which seems to be consistent with the localization of carriers at $T=0$ K as the CO ground state implies.

## V. BAND DISCONTINUITIES ACROSS THE INTERFACE

The GGA gap for bulk $SrTiO_3$ is 2.0 eV (experimental value 3.2 eV) separating filled O 2*p* bands and unfilled Ti 3*d* bands. Applying GGA+$U$ enhances the band gap to 2.7 eV, but does not influence the electronic behavior of the system (e.g., in terms of Ti 3*d* occupation). For $LaAlO_3$ we obtain a band gap within GGA of 3.7 eV (experimental value 5.6 eV) between filled O 2*p* bands hybridized with Al *p* bands and unfilled conduction bands comprised of La 5*d* and Al 3*s*, 3*p* states.

How the bulk band gaps line up across the interface is one of its most fundamental characteristics. Especially when "excess" charge must be accommodated at an interface, the relative positions of the valence-band maxima $E_v$ and conduction band minima $E_c$ may have a large impact on the charge distribution. In principle these band edges can be identified through the layer projected DOS in successive layers away from the interface.[7,27] However, valence and conduction wave functions, and the local DOS, can be relatively slow to approach their bulk values. A more efficient approach is to use core eigenvalues. The charge density, and hence the potential, reaches its bulk value more quickly than the Bloch wave functions, and hence the core eigenvalues attain their bulk values only a few layers from the interface.

In the current system the O 1*s* eigenvalues are the natural choice as they give an idea how the local potential changes across interface. Four cases are displayed in Fig. 4: both GGA and GGA+$U$ calculations, each with ideal and with relaxed atomic positions. We note that O 1*s* energies in the AO and $BO_2$ layers are distinct near the interface, and attain the (identical) bulk value already two or three layers from the interface. For the ideal geometry, this convergence is slower in GGA than in GGA+$U$ on the STO side, because in GGA the charge is accommodated over a few STO layers, while in GGA+$U$ the charge is localized at the interface.

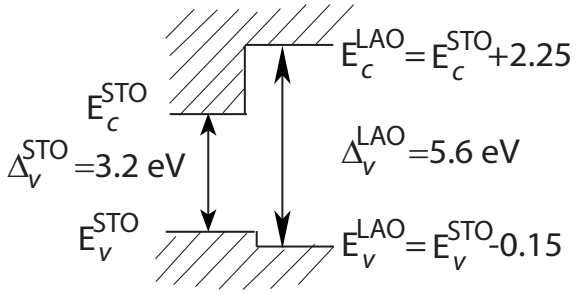


FIG. 5. Schematic picture of the band alignment at the *n*-type interface in the $LAO_{4.5}/STO_{5.5}$ superlattice calculated using the variation of the O 1*s* core levels across the interface and the experimental band gaps $\Delta_{STO}=3.2$ eV and $\Delta_{LAO}=5.6$ eV.

The overriding result is that relaxation, using either method, leads to a large decrease in the variations in positions of the O 1*s* core levels across the interface. Although the electronic behavior at the interface layer is very different, the O 1*s* energy difference $E_{1s}^{STO}-E_{1s}^{LAO}$ in the central (most distant from the interface showing bulklike behavior) layers in the STO and LAO part of the superlattice turn out to be identical both for GGA and GGA+$U$: the core levels are 0.20 eV higher in LAO than in STO.

From Fig. 4, the O 1*s* eigenvalues in the respective central LAO (STO) layers appear to have reached their asymptotic values and thus are expected to align with the corresponding level in a reference bulk system.[28] Hence, using the $E_v-E_{1s}$, extracted from a separate calculation for each bulk material, as well as $E_{1s}^{STO}-E_{1s}^{LAO}$ from the slab calculation discussed above, the valence-band alignment across the interface is determined as follows:

$$E_v^{LAO}-E_v^{STO}=[E_v^{LAO}-E_{1s}^{LAO}]+[E_{1s}^{LAO}-E_{1s}^{STO}]-[E_v^{STO}-E_{1s}^{STO}]. \quad (1)$$

To obtain the conduction band discontinuity, we correct for the underestimation of the band gaps within GGA, by using the experimental band gaps of $LaAlO_3$ and $SrTiO_3$:

$$E_v^{LAO}=E_v^{STO}-0.15 \text{ eV},$$

$$E_c^{LAO}=E_c^{STO}+2.25 \text{ eV}. \quad (2)$$

The schematic band lineup is pictured in Fig. 5. Because the STO band gap lies completely within the LAO band gap, charge carriers of either sign (electrons or holes) near the interface will go into the STO side of the IF.

It is clear from Fig. 4 that the band lineup is very sensitive to relaxation, but also other details of the calculation may play a role. For example, Albina *et al.*[7] used smaller simulation cells and a compensating background charge and re-

ported values of 0.3 to 0.5 eV depending on the number of layers in the supercell and the method: They applied both the macroscopic potential averaging technique and the local DOS, illustrating the difference these two methods can give. On the other hand, Lee and Demkov[29] reported a very similar valence-band offset (−0.1 eV) using the reference potential method.

## VI. SUMMARY

In summary, we find that the polar discontinuity at the isolated *n*-type LAO/STO interface is accommodated through an intricate combination of an ionic relaxation and an electronic reconstruction. The strong polar distortions lead to a reduction in the valence-band discontinuity at the interface compared to the ideal structure and partially compensate the excess charge. This appears to be consistent with the measured lower carrier density of $1.8\times10^{14}$ $cm^{-2}$ corresponding to ~0.27 instead of the expected 0.5 electrons per unit cell.[10] Charge accommodation at the isolated *n*-type interface requires occupation of the Ti 3*d* band. Within GGA $+U$ the ground state is a charge-ordered checkerboard arrangement of $Ti^{3+}$ ($d_{xy}$ orbital occupation) and $Ti^{4+}$ ions in the interface layer. Lattice relaxations within GGA lead to longer ranged and more pronounced relaxations, and to a suppression of charge order as the excess charge spreads over a few STO layers near the interface. The residual orbital polarization $d_{xy}$ in the interface $TiO_2$ layer and the degenerate Ti $t_{2g}$ bands in deeper layers may lead to interesting transport properties in this system.

## ACKNOWLEDGMENTS

We acknowledge helpful discussions with J. Mannhart, M. Huijben, and J. Eckstein and support through the Bavaria-California Technology Center (BaCaTeC), from DOE under Grant No. DE-FG03-01ER45876, and a grant for computational time at the supercomputer HLRBII at the Leibniz Rechenzentrum.

[1] A. Ohtomo and H. Y. Hwang, Nature (London) **427**, 423 (2004).
[2] A. Brinkman, M. Huijben, M. van Zalk, J. Huijben, U. Zeitler, J. C. Maan, J. G. van der Wiel, G. Rijnders, D. H. A. Blank, and H. Hilgenkamp, Nature Mater. **6**, 493 (2007).
[3] M. Vanzalk, J. Huijben, A. Giesbers, M. Huijben, U. Zeitler, J. Maan, W. Vanderwiel, G. Rijnders, D. Blank, H. Hilgenkamp, and A. Brinkman, arXiv:0806.4450 (unpublished).
[4] N. Reyren, S. Thiel, A. D. Caviglia, L. Fitting Kourkoutis, G. Hammerl, C. Richter, C. W. Schneider, T. Kopp, A.-S. Rüetschi, D. Jaccard, M. Gabay, D. A. Muller, J.-M. Triscone, and J. Mannhart, Science **317**, 1196 (2007).
[5] S. Gemming and G. Seifert, Acta Mater. **44**, 4299 (2006).
[6] M. S. Park, S. H. Rhim, and A. J. Freeman, Phys. Rev. B **74**, 205416 (2006).
[7] J.-M. Albina, M. Mrovec, B. Meyer, and C. Elsässer, Phys. Rev. B **76**, 165103 (2007).
[8] W. Siemons, G. Koster, H. Yamamoto, W. A. Harrison, G. Lucovsky, T. H. Geballe, D. H. A. Blank, and M. R. Beasley, Phys. Rev. Lett. **98**, 196802 (2007).
[9] N. Nakagawa, H. Y. Hwang, and D. A. Muller, Nature Mater. **5**, 204 (2006).
[10] M. Huijben, G. Rijnders, D. H. A. Blank, S. Bals, S. van Aert, J. Verbeeck, G. van Tendeloo, A. Brinkman, and H. Hilgenkanp, Nature Mater. **5**, 556 (2006).
[11] A. Kalabukhov, R. Gunnarsson, J. Borjesson, E. Olsson, T. Claeson, and D. Winkler, Phys. Rev. B **75**, 121404(R) (2007).
[12] M. Basletic, J.-L. Maurice, C. Carétéro, G. Herranz, O. Copie, M. Bibes, É. Jacquet, K. Bozehouane, S. Fusil, and A. Barthélémy, Nature Mater. **7**, 621 (2008).
[13] G. Rijnders and D. H. A. Blank, Nature Mater. **7**, 270 (2008).
[14] R. Pentcheva and W. E. Pickett, Phys. Rev. B **74**, 035112 (2006).
[15] Z. Zhong and P. Kelly, EPL **84**, 27001 (2008).
[16] R. Pentcheva and W. E. Pickett, Phys. Rev. Lett. **99**, 016802 (2007).
[17] P. Blaha, K. Schwarz, G. K. H. Madsen, D. Kvasnicka, and J. Luitz, *WIEN2k, An Augmented Plane Wave Plus Local Orbitals Program for Calculating Crystal Properties* (Karlheinz Schwarz, Techische Universitat Wien, Austria, 2001).
[18] J. P. Perdew, K. Burke, and M. Ernzerhof, Phys. Rev. Lett. **77**, 3865 (1996).
[19] V. I. Anisimov, I. V. Solovyev, M. A. Korotin, M. T. Czyzyk, and G. A. Sawatzky, Phys. Rev. B **48**, 16929 (1993).
[20] I. Solovyev, N. Hamada, and K. Terakura, Phys. Rev. B **53**, 7158 (1996).
[21] F. Tran, J. Kunes, P. Novak, P. Blaha, L. D. Marks, and K. Schwarz, Comput. Phys. Commun. **179**, 784 (2008).
[22] D. R. Hamann, D. A. Muller, and H. Y. Hwang, Phys. Rev. B **73**, 195403 (2006).
[23] S. Okamoto, A. J. Millis, and N. A. Spaldin, Phys. Rev. Lett. **97**, 056802 (2006).
[24] J.-L. Maurice, C. Carretero, M.-J. Casanove, K. Bouzehouane, S. Guyard, E. Larquet, and J.-P. Contour, Phys. Status Solidi A **203**, 2209 (2006).
[25] J.-L. Maurice, I. Devos, M.-J. Casanove, C. Carretero, G. Gachet, D.-G. Crete, D. Imhoff, A. Barthelemy, M. Bibes, K. Bouzehouane, C. Deranlot, S. Fusil, E. Jacquet, B. Domenges, and D. Ballutaud, Mater. Sci. Eng., B **144**, 1 (2007).
[26] K. Janicka, J. P. Velev, and E. Tsymbal, J. Appl. Phys. **103**, 07B508 (2008).
[27] M. Peressi, N. Blinggeli, and A. Baldareshi, J. Phys. D **31**, 1273 (1998).
[28] S. C. Erwin and W. E. Pickett, Solid State Commun. **81**, 891 (1992).
[29] J. Lee and A. A. Demkov, *Ferroelectrics and Multiferroics*, edited by V. Gopalan, J.-P. Maria, M. Fiebig, C.-W. Nan, MRS Symposia Proceedings No. 966 (Materials Research Society, Warrendale, PA, 2007), p. 0966–T07–33.